Voltage control of Ca^{2+} permeation through N-type calcium ($Ca_V2.2$) channels

Zafir Buraei,[1,2] Haoya Liang,[2] and Keith S. Elmslie[2,3]

[1]Department of Biology and Health Sciences, Pace University, New York, NY 10038
[2]Department of Physiology, Tulane University Health Sciences Center, New Orleans, LA 70112
[3]The Baker Laboratory of Pharmacology, Department of Pharmacology, Kirksville College of Osteopathic Medicine, A.T. Still University of Health Sciences, Kirksville, MO 63501

Voltage-gated calcium (Ca_V) channels deliver Ca^{2+} to trigger cellular functions ranging from cardiac muscle contraction to neurotransmitter release. The mechanism by which these channels select for Ca^{2+} over other cations is thought to involve multiple Ca^{2+}-binding sites within the pore. Although the Ca^{2+} affinity and cation preference of these sites have been extensively investigated, the effect of voltage on these sites has not received the same attention. We used a neuronal preparation enriched for N-type calcium ($Ca_V2.2$) channels to investigate the effect of voltage on Ca^{2+} flux. We found that the EC_{50} for Ca^{2+} permeation increases from 13 mM at 0 mV to 240 mM at 60 mV, indicating that, during permeation, Ca^{2+} ions sense the electric field. These data were nicely reproduced using a three-binding-site step model. Using roscovitine to slow $Ca_V2.2$ channel deactivation, we extended these measurements to voltages <0 mV. Permeation was minimally affected at these hyperpolarized voltages, as was predicted by the model. As an independent test of voltage effects on permeation, we examined the Ca^{2+}-Ba^{2+} anomalous mole fraction (MF) effect, which was both concentration and voltage dependent. However, the Ca^{2+}-Ba^{2+} anomalous MF data could not be reproduced unless we added a fourth site to our model. Thus, Ca^{2+} permeation through $Ca_V2.2$ channels may require at least four Ca^{2+}-binding sites. Finally, our results suggest that the high affinity of Ca^{2+} for the channel helps to enhance Ca^{2+} influx at depolarized voltages relative to other ions (e.g., Ba^{2+} or Na^+), whereas the absence of voltage effects at negative potentials prevents Ca^{2+} from becoming a channel blocker. Both effects are needed to maximize Ca^{2+} influx over the voltages spanned by action potentials.

INTRODUCTION

Voltage-gated calcium (Ca_V) channels are involved in processes ranging from neurotransmitter release to cardiac muscle contraction, and mutations in Ca_V channels have been shown to cause diseases including migraines, autism, epilepsy, and cardiac insufficiency (Bidaud et al., 2006; Catterall et al., 2008; Liao and Soong, 2010; Rajakulendran et al., 2012; Schmunk and Gargus, 2013). One function of voltage-gated channels is to produce changes in membrane voltage. However, Ca_V channels have an additional function, which is to deliver the second messenger Ca^{2+} into the cell. Thus, the mechanism by which these channels selectively allow the permeation of Ca^{2+} has been a burning question for several decades. Ca^{2+} has micromolar affinity for the Ca_V channel pore in which it functions as a blocker of Na^+ and K^+ flux through these channels (Almers and McCleskey, 1984; Hess et al., 1986; Rosenberg and Chen, 1991). However, such a strong affinity should preclude Ca^{2+} permeation of the channel. Several models emerged to explain this paradox, which postulate the existence of a high-affinity site in tandem with one or more low-affinity sites in the channel pore. These additional sites overcome the Ca^{2+} block by either disrupting the bound Ca^{2+} via a repulsion mechanism (Hess and Tsien, 1984) or forcing the blocking Ca^{2+} to move inward along lower-affinity binding sites (Dang and McCleskey, 1998). These models were developed for L-type ($Ca_V1.2$) channels, but their predictions have not been fully tested, nor were they tested for other Ca_V channels such as N-type ($Ca_V2.2$) channels. In addition, the impact of voltage on permeation has not been completely explored for any Ca_V channels, yet Ca^{2+} influx through these channels most often occurs in the context of changing voltages such as those generated by action potentials.

Most of the information on the voltage control of ions in the Ca_V channel pore comes from studies in which a monovalent cation (e.g., Na^+) was used as the permeating ion, while divalent cations (e.g., Ca^{2+}) were used as the blocking ion (Almers et al., 1984; Hess et al., 1986; Rosenberg and Chen, 1991; Kuo and Hess, 1993a). The ability of micromolar Ca^{2+} or Ba^{2+} to block Na^+ currents shows that the calcium channel pore has a high-affinity

Correspondence to Keith S. Elmslie: kelmslie@atsu.edu

Abbreviations used in this paper: AMFE, anomalous MF effect; Ca_V, voltage-gated calcium; MA, methylamine; MF, mole fraction.

The Rockefeller University Press $30.00
J. Gen. Physiol. Vol. 144 No. 3 207–220
www.jgp.org/cgi/doi/10.1085/jgp.201411201

binding site for divalent cations (Almers and McCleskey, 1984; Hess and Tsien, 1984; Dang and McCleskey, 1998). Furthermore, the ionic block at the high-affinity site is voltage dependent with depolarization increasing the off-rate of the blocking ion. This indicates that ions at that site sense the transmembrane electrical field (Hess et al., 1986; Thévenod and Jones, 1992; Carbone et al., 1997; Block et al., 1998).

In contrast, studies that have focused on permeation have shown that voltage has little or no effect on the movement of ions within the Ca_V channel pore. Kuo and Hess (1993b) found that changes in transmembrane voltage failed to alter the impact of divalent cations, like Ba^{2+}, on the off rate of another divalent cation (e.g., Cd^{2+}) from the $Ca_V1.2$ channel high-affinity site. Voltage also had little or no impact on the Na^+ block of current generated by Ca^{2+} through $Ca_V2.2$ channels (Polo-Parada and Korn, 1997). Permeation of $Ca_V3.1$ channels was examined over a wide voltage range (−120 to 30 mV) and found to have little or no voltage dependence (Khan et al., 2008).

The apparent difference in voltage dependence between the blocking and permeation sites might suggest that only the blocking site is located within the electric field. One possibility is that large distances separate the blocking and permeation sites. However, this is at odds with the recent crystal structure, which shows several adjacent Ca^{2+}-binding sites within a Ca^{2+}-permeant Na_V channel (Tang et al., 2014). Alternatively, the apparent absence of a voltage effect on permeation could suggest a very steep voltage gradient within the pore that includes only the high-affinity blocking site. One problem is that most of the permeation studies have previously focused on voltages <0 mV (Kuo and Hess, 1993b,c; Polo-Parada and Korn, 1997), whereas the blocking studies have used a wider range of voltages (Hess et al., 1986; Thévenod and Jones, 1992; Carbone et al., 1997; Block et al., 1998). In addition, evidence from both simulation and anomalous mole fraction (MF) effect (AMFE) studies support an effect of voltage on permeation of $Ca_V1.2$ channels at voltages ≥0 mV (Campbell et al., 1988; Friel and Tsien, 1989).

Here we examine the effect of voltage on the permeation of Ca^{2+} and Ba^{2+} through $Ca_V2.2$ channels using permeation affinity measurements, anomalous MF, and computer simulations. We find that voltage impacts the apparent affinity of these ions for both blocking and permeating the channel with the strongest effects at voltages >0 mV. These experimental data were used to provide parameters for the three-binding-site step model of Dang and McCleskey (1998), which was able to fit the effect of voltage on Ca^{2+} permeation. However, we could not find parameters that would reproduce the concentration and voltage dependence of AMFE between Ca^{2+} and Ba^{2+}. The AMFE data were reproduced after we added a fourth site to the model. Based on our model, we conclude that four Ca^{2+}-binding sites are required to produce Ca^{2+} and Ba^{2+} flux through $Ca_V2.2$ channels, which is consistent with the recent structural information from a calcium channel pore engineered in a bacterial voltage-gated sodium channel (Tang et al., 2014).

MATERIALS AND METHODS

Cells

Adult bullfrogs (*Rana catesbeiana*) were chilled to 4°C, brain pithed, decapitated, and spine pithed before the paravertebral sympathetic ganglia were removed. The method of sacrifice was approved by the Institutional Animal Care and Usage Committee. Neurons were dissociated with collagenase/dispase digestion and trituration (Kuffler and Sejnowski, 1983; Jones, 1987; Elmslie et al., 1992). Cells were maintained for 1–14 d at 4°C in L-15 medium supplemented with 10% fetal bovine serum and penicillin/streptomycin.

Recordings

Neurons were voltage clamped in the whole-cell configuration using an Axopatch 200A amplifier (Molecular Devices). Capacitance and series resistance (ranging from 0.3 to 4 MΩ) were compensated 80–85%. Experiments were controlled with a Macintosh II computer (Apple Inc.) running S3 data acquisition software written by S. Ikeda (National Institute on Alcohol Abuse and Alcoholism, National Institutes of Health, Bethesda, MD). Currents were digitized with a MacAdios II analogue-digital converter (GW Instruments) and stored on hard disk. Leak currents were subtracted using a −P/4 protocol. Voltage steps were 10 ms in length unless otherwise noted. Step and tail currents were sampled at 50 Hz and they were typically filtered at 5 kHz. All recordings were performed at room temperature (24°C). Pipettes were pulled from Schott 8250 glass (Garner Glass Co.) on a P-97 puller (Sutter Instrument).

Data analysis

Data were analyzed using Igor Pro (WaveMetrics) running on a Macintosh computer. The step current was measured as the mean of 10 points at the end of a 10-ms voltage step. Tail currents were measured as the mean of three to five points beginning 300 µs from the end of the step current.

The affinity (K_d) of ion binding to a certain site will change with voltage if the binding site is located in the electrical field. From the trend of those changes in K_d with voltage, the electric distance (the fraction of electrical field sensed $1 > \delta > 0$) of the binding site can be calculated according to the Woodhull equation (Woodhull, 1973):

$$K_d(0) / K_d(V) = \exp\left[(-zF/RT)V\delta\right], \quad (1)$$

where $K_d(0)$ and $K_d(V)$ are the apparent K_d at membrane potential 0 mV and any given voltage V, respectively. F, R, and T are Faraday's constant, the gas constant, and the temperature in kelvin, respectively. δ is the fractional electrical field sensed at the binding site, and z is the valence of the ion that binds to the site. Because measured EC_{50} was our best estimate of K_d, we substituted EC_{50} for K_d in the Woodhull equation.

Solutions

To isolate Ca^{2+} currents, Na^+ and K^+ were replaced in the internal and external solutions with the impermeant cation NMDG. NMDG has been shown to provide better Ca_V current isolation than inorganic monovalent cations (Jones and Marks, 1989), but some data can be interpreted as external NMDG producing a small block of $Ca_V2.2$ channels (IC_{50} = 320 mM; Zhou and Jones, 1995). However, the impact of this small effect on our results should be minimal

because our maximum NMDG concentration is 115 mM. The internal solution (pH 7.2) contained (mM) 61.5 NMDG-Cl, 6 $MgCl_2$, 14 creatine phosphate, 2.5 NMDG-HEPES, 5 Tris-ATP, 10 NMDG-EGTA, and 0.3 Li GTP. The extracellular solution contained (mM) 110 NMDG-Cl, 10 NMDG-HEPES, and 3 $CaCl_2$. For experiments requiring higher divalent cation concentrations, 3 mM Ca^{2+} was replaced by 10, 30, or 100 mM $CaCl_2$, and the NMDG-Cl concentration was reduced to maintain osmolarity. Some experiments were performed using 300 mM Ca^{2+} in which NMDG-Cl was replaced by 300 mM $CaCl_2$. We did not attempt to adjust other solutions to match the high osmolarity of the 300 mM Ca^{2+} solution, but this solution was applied for only short durations because the Ca_V current declined with continued application. We did not investigate the source for this decline, but possible reasons include (a) Ca^{2+}-dependent inactivation of $Ca_V2.2$ channels (Liang et al., 2003; Goo et al., 2006), as the high $[Ca^{2+}]_i$ overwhelms the buffering capacity of EGTA, and (b) the high osmolarity of the external solution negatively impacting the recording. Except for 300 mM Ca^{2+}, the osmolarity of the external solutions was 240 mOsm and that for the internal solution was 200 mOsm. All solutions were titrated to pH 7.2 with NMDG-base. The AMFE measures the interference of one permeant ion with the permeation of another permeant ion. We investigated AMFE between Ca^{2+} and Ba^{2+} by mixing external solutions containing the same concentration of either Ca^{2+} or Ba^{2+} to obtain Ba^{2+} MFs of 0, 0.3, 0.7, 0.9, and 1. For these experiments, $CaCl_2$ was replaced by an equal concentration of $BaCl_2$.

Some experiments examined divalent cation block of monovalent cation current through $Ca_V2.2$ channels. For these experiments, methylamine (MA) was used as the charge carrier because it does not permeate sodium or potassium channels and, thus, provides excellent isolation of $Ca_V2.2$ current (Liang and Elmslie, 2002). The extracellular solution contained (mM) 90 MA-Cl, 10 NMDG-HEPES, and 10 nM HEDTA, and the $CaCl_2$ concentration was varied to obtain the desired free Ca^{2+} concentration. The total Ca^{2+} concentration ($[Ca^{2+}]_o$) was calculated from the desired free $[Ca^{2+}]_o$ and the stability constant of HEDTA (Martell and Smith, 1974) using computer programs based on Fabiato and Fabiato (1979). These solutions were titrated to pH 7.2 with NMDG-base, and the osmolarity ranged from 220 to 250 mOsm.

Limitation of this dataset

There are two problems that could negatively impact our permeation data. One is poor voltage control and the other is $Ca_V2.2$ current isolation. Good membrane voltage control is an issue that requires constant attention when patch clamping. Voltage control can be degraded when currents become large and fast, as when tail currents are measured at high divalent cation concentrations (Zhou and Jones, 1995). To guard against poor voltage control, we used low resistance electrodes that yielded series resistances ranging from 0.3 to 4 MΩ and compensated the series resistance by 80–85%. We also monitored the tail currents to ensure monophasic deactivation kinetics as expected from proper voltage control (Jones, 1990).

The second potential problem was isolation of $Ca_V2.2$ current. The Ca_V current in bullfrog sympathetic neurons is comprised of 90–95% $Ca_V2.2$ (N-type) current when recorded in 3 mM Ba^{2+} (Jones and Marks, 1989; Elmslie et al., 1992), but 75% when recorded in 3 mM Ca^{2+} (Liang and Elmslie, 2001). The difference between Ca^{2+} and Ba^{2+} results from the increased impact of a $Ca_V2.3$-like current that we call E_f current (Liang and Elmslie, 2001). E_f current is more prominent in Ca^{2+} and at high divalent cation concentrations (Elmslie et al., 1994; Liang and Elmslie, 2001). Thus, as Ca^{2+} concentration increases, the fraction of Ca_V current generated by $Ca_V2.2$ channels decreases. One method to address this problem would be to block E_f current using Ni^{2+}, which is the only known blocker. However, there is no Ni^{2+} concentration that would block the majority of E_f current without affecting $Ca_V2.2$ (Liang and Elmslie, 2001). In addition, Ni^{2+} block is dependent on both $[Ca^{2+}]_o$ and voltage (Zamponi et al., 1996) so that block will change as we altered these parameters to investigate permeation. Based on previous work, we estimate that impact of E_f current varies from 12 to 25% of the total Ca_V current when changing from 3 to 100 mM $[Ca^{2+}]_o$ (Liang and Elmslie, 2001), which suggests that $Ca_V2.2$ current dominates even at high $[Ca^{2+}]_o$. For this reason, we believe that our permeation data primarily reflect the activity of $Ca_V2.2$ channels.

Modeling

The three-site model was written in SCOP (Simulation Resources, Inc.) by S. Jones (Case Western Reserve University, Cleveland, OH) based on that published by Dang and McCleskey (1998). The model has three energy wells and four barriers (Fig. 1). Their depths and heights, respectively, are constrained by some experimental data. Lansman et al. (1986) demonstrated that Ca^{2+} enters the pore at a rate of $\sim 10^9$/M/s, the value expected from diffusion-limited ion movement. Thus, the two external barriers were set to ≥8.6 kT (Almers and McCleskey, 1984). In addition, model parameters were set to give reasonable single-channel current amplitudes of ~1.5 pA at 0 mV in 100 mM Ba^{2+} (Yue and Marban, 1990; Elmslie, 1997).

Well depth values were obtained from experimental data from $Ca_V2.2$ channels. Those data for Ca^{2+} are presented here, but data for Ba^{2+} came from other publications. The Ba^{2+} EC_{50} for permeation at 0 mV was obtained from Zhou and Jones (1995), whereas the IC_{50} for Ba^{2+} block of monovalent current was from Liang and Elmslie (2002). The values for the high-affinity binding site were set using the IC_{50} for block of monovalent cations, whereas the EC_{50} for permeation was used to set the values for the enhancement sites (Fig. 1). At 0 mV, the electrical field does not affect ion movement. Therefore, we used data from this voltage to set well depths. For simplicity, the well depths for the two enhancement sites were identical in the three-site model (Dang and McCleskey, 1998).

The model calculates current based on ion movement across each barrier, which depends on the barrier height and well depth, electrical distance, and applied voltage. Ion concentration only affects the rates of entering into the first well from outside and

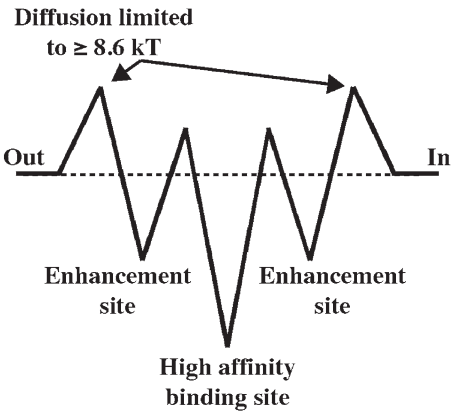

Figure 1. Diagram of the Dang and McCleskey three-site model. The model shows the energy barriers and wells of the three-site model along with labels that define the wells. The internal and external barriers are set to limit entry into the pore and exit from the pore by the rate of diffusion (Almers and McCleskey, 1984). The depth of the high-affinity binding site was estimated from the EC_{50} for Ca^{2+} block at 0 mV, whereas the depth of the enhancement sites was estimated from the EC_{50} for Ca^{2+} permeation at 0 mV (see Results).

the third well from inside (Fig. 1). Here is the example for calculating rates of "hopping" over the first barrier:

$$k1a = [a]_o * kTh * \exp(-\text{barrier height}) * \exp(-z_A * mV * d1/RTF)$$
$$km1a = kTh * \exp(\text{well depth} - \text{barrier height}) * \exp(z_A * mV * dm1/RTF),$$

where k, T, h, R, and F have their usual thermodynamic meanings, $[a]_o$ is concentration of ion "a" outside, mV is the applied voltage, z_A is the charge of ion "a," and d1 is the electrical distance of the first well. k1a is the forward rate constant (moving into the channel), whereas km1a is the backward rate constant over the same barrier (moving out of the channel).

Online supplemental material

Contents include two figures showing how repulsion diminishes or abolishes the concentration dependence of AMFE. The three-well, four-barrier model was used, and the energy profiles for Ba^{2+} and Ca^{2+} in Fig. S1 were based on physiologically relevant block and permeation values. Fig. S2 shows results from another simulation using repulsion with an altered Ba^{2+} energy profile in an attempt to improve the fits by altering parameters. Online supplemental material is available at http://www.jgp.org/cgi/content/full/jgp.201411201/DC1.

RESULTS

Ca^{2+} block

As a first step toward determining the permeation properties of the $Ca_V2.2$ channel, we examined the Ca^{2+} block of monovalent cation current (MA^+; see Materials and methods; Fig. 2). The blocking $[Ca^{2+}]_o$ ranged from 0.03 to 100 µM, and step voltages ranged from −40 to 80 mV. As shown in Fig. 2 (A and B), progressively increasing $[Ca^{2+}]_o$ produced larger block of monovalent cation current at −20 mV that reached a maximum at 30 µM. When measured at different step voltages, both the affinity for Ca^{2+} and maximum block changed. The affinity for Ca^{2+} decreased with depolarization (EC_{50} for block increased), whereas the maximum block decreased (Fig. 2, C and D). For example, the EC_{50} changed from 0.2 µM at −40 mV to 2.5 µM at 80 mV, and the maximum block decreased from 87 ± 7% at −40 mV to 24 ± 6% at 80 mV. Both of these changes are consistent with the idea that Ca^{2+} ions sense the transmembrane voltage when occupying the high-affinity blocking site. We estimated

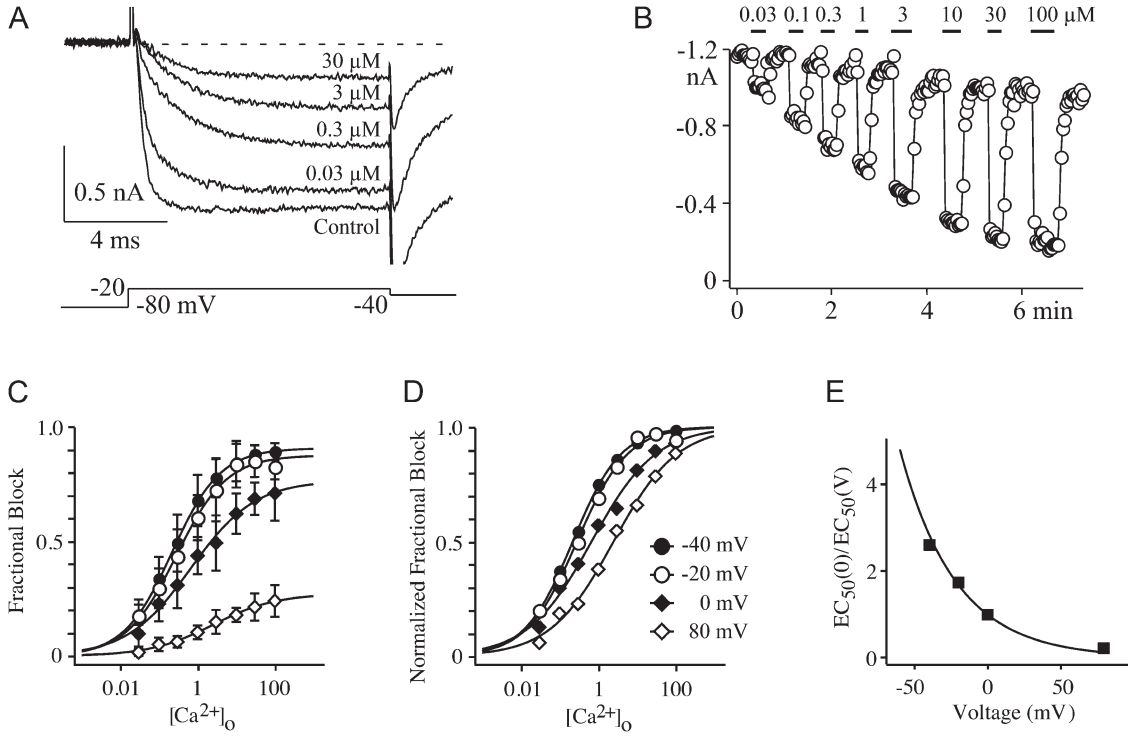

Figure 2. Ca^{2+} block of $Ca_V2.2$ step currents. (A) Step current traces are shown for control and four different $[Ca^{2+}]_o$ as indicated. The charge carrier for these Ca^{2+} blocking experiments was MA^+. (B) The time course of block at −20 mV by Ca^{2+} at the indicated concentrations. The black bars indicate when Ca^{2+} was applied. (C) The Ca^{2+} block dose–response relationship is altered by step voltage. The mean fractional block (±SD) from 3–14 neurons is plotted versus $[Ca^{2+}]_o$ for voltages ranging from −40 to 80 mV as indicated in D. The solid lines are the fits of the fractional block using the Hill equation. The EC_{50} at each of the four different voltages is (µM) 0.2 (−40 mV), 0.3 (−20 mV), 0.7 (0 mV), and 2.5 (80 mV). (D) To better illustrate the shift in EC_{50}, the data shown in C was replotted after normalization to maximum block as determined from fitting the data using the Hill equation. The EC_{50} values are the same as those listed for C. (E) The ratio of EC_{50} at 0 mV divided by that at a given voltage (V; $EC_{50}(0)/EC_{50}(V)$) is plotted versus step voltage. The smooth line is a fit to these data using the Woodhull equation (Eq. 1), which yielded an electrical distance for the blocking site of 0.34.

the electrical distance of the Ca^{2+} blocking site using the Woodhull equation (Eq. 1), which yielded a relative electrical distance (∂) of 0.34 for Ca^{2+} entering from the extracellular side of the pore (Fig. 2 E).

Ca^{2+} permeation is voltage dependent

The impact of voltage on permeation has yet to be experimentally investigated at voltages >0 mV, so we wanted to measure the Ca^{2+} EC_{50} for permeation at different voltages. However, changing $[Ca^{2+}]_o$, which is required to determine the EC_{50}, will also affect the gating of Ca_V channels (Brink, 1954; Hille, 1992). This dual effect was revealed by examination of current-voltage (I-V) relationships in different $[Ca^{2+}]_o$ (Fig. 3). With each increase in $[Ca^{2+}]_o$, the current increased because of the larger driving force on Ca^{2+}, but the peak of the I-V shifts to more depolarized voltages as a result of surface charge screening by divalent cations (Zhou and Jones, 1995). Thus, step current measurements do not isolate the Ca^{2+} effects on permeation from the gating effects. Because of this mixed effect, the peak step current measurements do not give an accurate estimate of Ca_V channel permeation (Zhou and Jones, 1995).

Tail currents can be used to isolate gating from permeation when changing $[Ca^{2+}]_o$ because the tail currents are measured at the same voltage regardless of $[Ca^{2+}]_o$ (Zhou and Jones, 1995; Wang et al., 2005). Using a step voltage of 100 mV to fully activate the $Ca_V2.2$ channels at all $[Ca^{2+}]_o$, we measured tail current at 0 mV in different $[Ca^{2+}]_o$ and calculated an EC_{50} = 16 mM (Fig. 4). In separate neurons, we conducted similar experiments while altering the tail voltage to determine whether the EC_{50} for permeation is voltage dependent (Fig. 5).

The plot of normalized tail current amplitude versus $[Ca^{2+}]_o$ shows that Ca^{2+} permeation of $Ca_V2.2$ channels changes with voltage (Fig. 5). The tail current amplitude at 0 mV reached a maximum at 100 mM Ca^{2+}, whereas that at 40 and 60 mV was clearly smaller in 100 versus 300 mM Ca^{2+}. This observation is borne out by fitting the data using the mass action equation, which yielded an EC_{50} = 13 mM for 0 mV versus 71 mM for 40 mV. The EC_{50} was even larger for 60 mV (240 mM; Fig. 5, B and C). The EC_{50} showed a monotonic increase with voltage, which further supports voltage-dependent interaction of Ca^{2+} with the $Ca_V2.2$ channel during permeation (Fig. 5, B and C). In an effort to more stringently test the voltage dependence of permeation hypothesis, we attempted to fit dose–response curves at different voltages

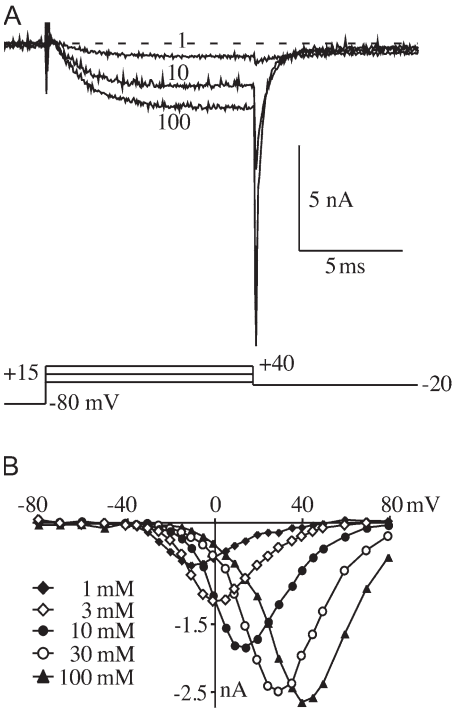

Figure 3. The effect of increasing $[Ca^{2+}]_o$ on whole-cell step current. (A) The three current records were recorded from the same neuron in 1, 10, and 100 mM Ca^{2+}. The selected voltages are those that generated peak current at the respective $[Ca^{2+}]_o$. (B) The I-V relationship in 1, 3, 10, 30, and 100 mM Ca^{2+}. Step currents were plotted versus the applied step voltage.

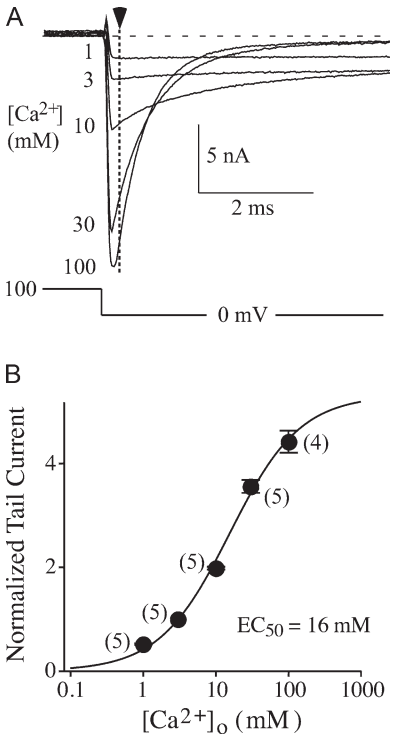

Figure 4. The current-concentration relationship measured from tail currents at 0 mV. (A) Tail currents were generated by repolarization to 0 mV after a conditioning step to 100 mV. Current traces in 1, 3, 10, 30, and 100 mM Ca^{2+} are shown. The vertical dashed line indicates where the tail currents were measured. (B) Peak tail current measurements from four to five neurons were averaged and plotted versus $[Ca^{2+}]_o$. The number of neurons used to generate each point is indicated, and the error bars show SD. The solid curve is a fit using the Hill equations to yield the indicated EC_{50}. The Hill coefficient was 0.9.

with Hill equations using the same EC_{50} but different K_{MAX} values, but this effort was unsuccessful. Thus, Ca^{2+} permeation of $Ca_V2.2$ channels appears to be strongly voltage dependent at voltages ≥0 mV.

We ran simulations using the three-site well and barrier or step permeation model (Dang and McCleskey, 1998) to determine whether this model could fit our experimental data. This model has two low-affinity sites that flank a high-affinity site (Fig. 1), which essentially function to enhance the off rate of bound ions (enhancement sites). The well depth for the high-affinity site was set to the EC_{50} for Ca^{2+} block of monovalent current at 0 mV (0.7 µM; Fig. 2), whereas the depth of the flanking enhancement wells was set using the permeation EC_{50} at 0 mV (13 mM; Fig. 4). We used the values at 0 mV to exclude the effect of transmembrane voltage. The position of these wells within the electric field was adjusted to match the voltage dependence of Ca^{2+} block and permeation EC_{50}. With a single set of parameters (Fig. 5 legend), the model could reproduce the voltage dependence of permeation. Fig. 5 C shows dose–response curves (lines) fit to simulated data points (small symbols) that also successfully reproduce the experimental data (large symbols) at all voltages.

We then used the model to predict the Ca^{2+} EC_{50} at voltages <0 mV (Fig. 5 C). At these voltages and high $[Ca^{2+}]_o$, the $Ca_V2.2$ channels deactivate too rapidly to permit accurate measurements of tail current amplitude. Surprisingly, the results showed smaller changes in EC_{50} with voltages <0 mV compared with voltages >0 mV with only a slight difference in the EC_{50} values at −40 versus −60 mV (2.9 vs. 2.3 mM, respectively). Thus, the step model of permeation, with a single set of parameters, predicts minimal voltage dependence of permeation at voltages <0 mV and strong voltage dependence of permeation at voltages >0 mV (Campbell et al., 1988).

As a test of this model prediction, we needed to overcome the limitations imposed by fast deactivation to examine permeation at voltages <0 mV. We used roscovitine to slow N-channel deactivation sufficiently to allow the tail measurement at voltages <0 mV (Buraei et al., 2005, 2007; Yarotskyy and Elmslie, 2009). Initially, we had to exclude the possibility that roscovitine affects permeation. Therefore, we compared permeation at voltages ≥0 mV

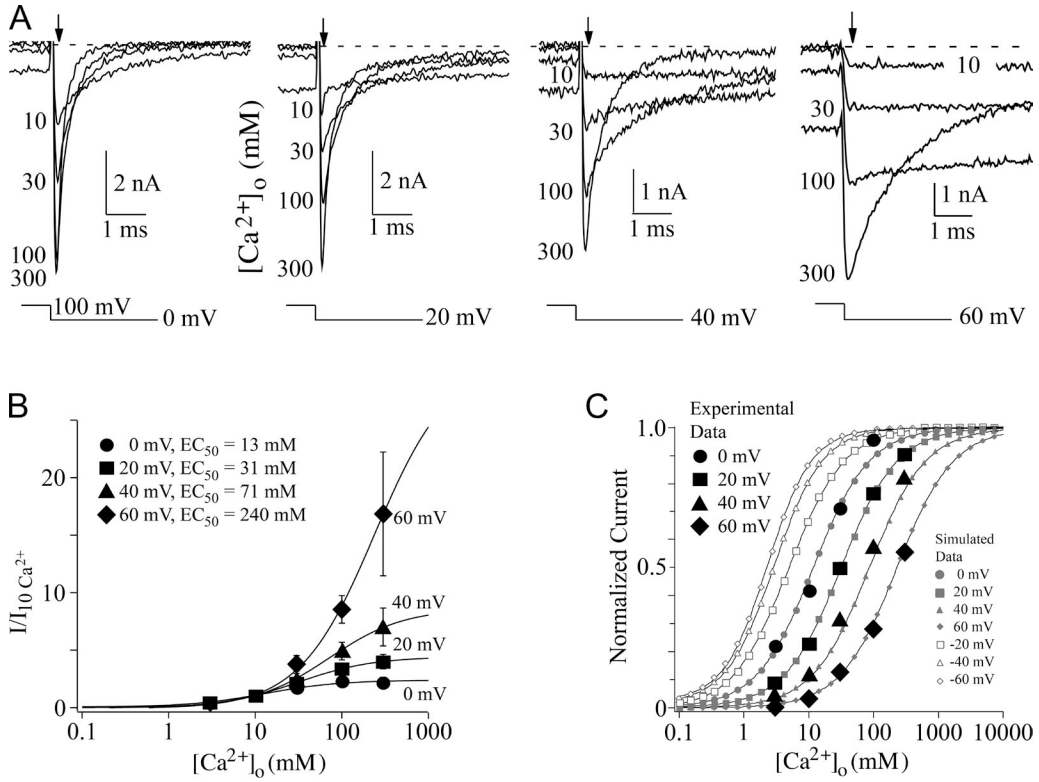

Figure 5. The voltage dependence of $Ca_V2.2$ channel permeation. (A) Tail currents at different voltages after depolarization to 100 mV are shown in the indicated $[Ca^{2+}]_o$. The arrows show where measurements were made to generate the dose–response curves in B. (B) Tail current amplitudes were normalized to those in 10 mM Ca^{2+} and plotted (mean ± SD) against the $[Ca^{2+}]_o$ for the indicated voltages. The dose–response curves for each tail voltage were fit using the mass-action equation to yield the indicated EC_{50} for Ca^{2+} permeation ($n = 9$–14). (C) The experimental data points (solid black symbols) from B and simulated data points from the three-site model (small gray symbols) were normalized to the maximum current determined from the mass-action fit of the simulated data. The EC_{50} for the simulated data were (mM) 2.3 (−60 mV), 2.9 (−40 mV), 4.9 (−20 mV), 12 (0 mV), 31 (20 mV), 86 (40 mV), and 238 (60 mV). Model parameters (Ca^{2+}) from outside to inside were (in kT) 8.7, −1, −1, and 9.6 for the barriers and −4.6, −14.7, and −4.6 for the wells. The fractional electrical distances for the wells were (unitless) 0.45, 0.5, and 0.9 (0.25, 0.8, and 0.9 gave similar results).

with (Fig. 6) versus without (Fig. 5) roscovitine to determine whether EC_{50} values were altered. The EC_{50} values obtained in roscovitine were similar to those without roscovitine. For example, at 0 mV, the EC_{50} = 20 versus 13 mM, and at 40 mV, EC_{50} = 90 versus 71 mM for roscovitine versus nonroscovitine datasets (Fig. 6). Thus, it appears that roscovitine does not modulate N-channel permeation.

One observation is that the EC_{50} in roscovitine was consistently larger than that in control (compare Fig. 5 with Fig. 6). Although we do not believe that roscovitine modulates permeation, this difference could result from the slower tail currents in roscovitine providing more accurate measurements at hyperpolarized voltages. Another possibility is variability from one dataset to another. Either way, the differences are fairly small, and the voltage dependence of permeation at voltages >0 mV is clear from both the control (Fig. 5) and roscovitine data (Fig. 6).

Because we validated the use of roscovitine to study $Ca_V2.2$ channel permeation, we measured EC_{50} at voltages <0 mV. As predicted, the Ca^{2+} dose–response curves at voltages <0 mV showed smaller changes with voltage (Fig. 6). For example, the change in EC_{50} from 0 to −20 mV was 4 mM (20 to 24 mM, respectively), whereas the change from 0 to 20 mV was 28 mM (20 to 48 mM, respectively). One obvious difference between our roscovitine experimental data and our simulated results (Fig. 5 C) was that the experimental EC_{50} values were much larger (Fig. 6). For example, at −40 mV our experimental EC_{50} = 31 mM was 10-times larger than the EC_{50} = 2.9 mM from the simulated data. Although the model correctly predicted the smaller change in EC_{50} with voltage at voltages <0 mV, the discrepancy with the experimental values suggests that different model parameters may be needed.

Electrical distance of the enhancement site

The data show an effect of voltage on permeating Ca^{2+} ions, which supports the placement of the enhancement (or permeation) sites of the model within the electrical field (Fig. 1). As with the Ca^{2+} blocking data, we used the Woodhull equation (Eq. 1) to estimate the electrical distance of the enhancement site (Woodhull, 1973). Fig. 7 shows the relative change in EC_{50} with voltage for Ca^{2+} permeation for data with and without roscovitine. Because the Woodhull equation (Eq. 1) returns a monotonic change in relative EC_{50} versus voltage, we fit only the data at voltages ≥0 mV (Fig. 7) to yield an electrical distance (∂) of ∼0.55 for permeating Ca^{2+} ions entering from extracellular side of the channel. This ∂ value is larger than that for the high-affinity site that was obtained from Ca^{2+} blocking data (∂ = 0.34). Thus, it seems likely that the ∂ value for permeation includes the electrical distances from multiple Ca^{2+}-binding sites. One way to study multiple binding sites in ion channel pores is by studying the AMFE.

AMFE

AMFE is defined as the occurrence of smaller currents in the presence of a mixture of two permeant ionic species, as compared with the currents in the presence of either one alone (Almers and McCleskey, 1984; Hess and Tsien, 1984; Hille, 1992). AMFE has been demonstrated in Ba^{2+}/Ca^{2+} mixtures for both $Ca_V1.2$ (Almers and McCleskey, 1984; Hess and Tsien, 1984; Friel and Tsien, 1989) and $Ca_V2.2$ channels (Wakamori et al., 1998). Thus, AMFE data can provide an independent dataset with which to probe the concentration and voltage dependence of permeation, as well as our permeation model (Fig. 5). As we did with Ca^{2+} permeation, we measured tail currents to examine AMFE so that

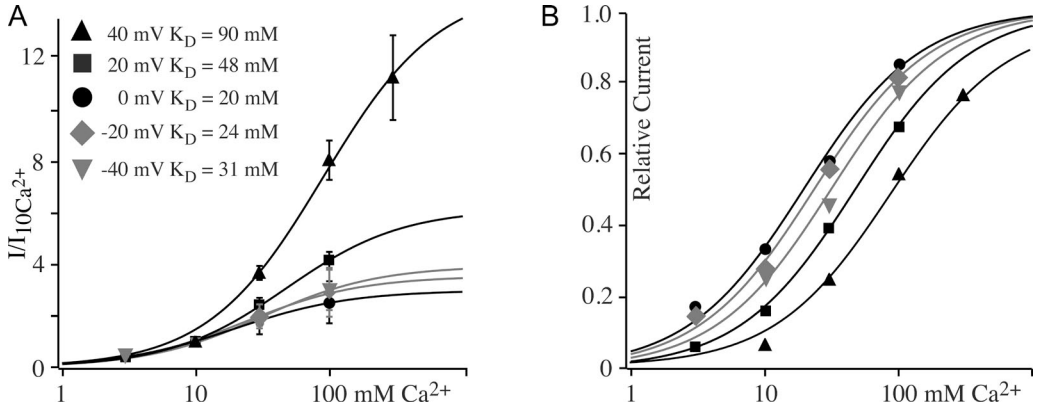

Figure 6. Little or no change in Ca^{2+} permeation EC_{50} at V < 0 mV. (A) The tail currents in 100 µM roscovitine were normalized to the current in 10 mM Ca^{2+} and plotted versus $[Ca^{2+}]_o$. The points of the dose–response curves are mean ± SD measured from 6–13 neurons. For a given $[Ca^{2+}]_o$, the points at −20 and −40 are not significantly different from each other but are different from those at 20 mV ($P < 0.05$). The data from each tail voltage were fit using the mass-action equation to yield the indicated EC_{50} values for Ca^{2+} permeation. (B) To better visualize the data, the dose–response curves in roscovitine (from A) were normalized to the maximum current values calculated from the mass-action fits to the experimental data. The symbols have the same meaning as in A.

permeation/block would be isolated from gating effects. While keeping the total ionic strength of the solutions equal, the MFs used for this study were 0, 0.1, 0.3, 0.7, 0.9, and 1, which corresponded to solutions with 0, 10, 30, 70, 90, and 100% Ba^{2+}, with the balance coming from Ca^{2+}. Fig. 8 shows an example of AMFE in a total Ba^{2+} + Ca^{2+} = 10 mM at a tail voltage of 20 mV. The current is the smallest at MF = 0.7 (70% Ba^{2+} + 30% Ca^{2+}). Note also that the current in 100% Ba^{2+} (MF = 1) is roughly 1.3-times larger than that in 100% Ca^{2+} (MF = 0; Fig. 8).

The concentration dependence of AMFE was studied using total divalent cation concentrations of 3, 10, and 30 mM and the same six MFs listed above. By limiting the maximum divalent cation concentration to 30 mM, we were able to resolve tail currents down to −20 mV. Fig. 9 presents AMFE data normalized to the current in MF = 0 (100% Ca^{2+}).

There are several general themes that can be gleaned from the AMFE data. First, for any given divalent cation concentration (3, 10, or 30 mM), the largest AMFE (minimal current) is observed at the most depolarized voltage (40 mV for these data; Fig. 10). Second, for any given voltage, the largest AMFE (minimal current) is observed at the lowest divalent cation concentration (3 mM for these data). Thus, the deepest AMFE minimum was found in 3 mM divalent cations at 40 mV. In contrast, there are relatively few conditions that yielded AMFE at divalent cations = 30 mM, which occurred at the most depolarized voltage (40 mV). Thus, it is clear from these data that AMFE of $Ca_V2.2$ channels is both concentration and voltage dependent.

One observation that has been consistently made when recording from both $Ca_V1.2$ and $Ca_V2.2$ currents is that the current in Ba^{2+} is larger than that in Ca^{2+} (Almers and McCleskey, 1984; Hess and Tsien, 1984; Liang and Elmslie, 2001; Goo et al., 2006). Although Fig. 10 shows this is the case for most voltages and divalent cation concentrations, three remarkable exceptions are shown. In 3 mM divalent cations at 40 mV, the Ca^{2+} current (MF = 0) is larger than the Ba^{2+} current (MF = 1), whereas the two currents are roughly equal at 20 mV.

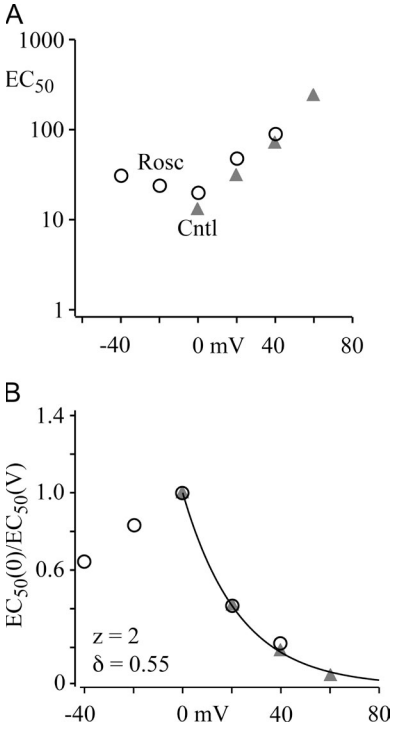

Figure 7. The electrical distance of the enhancement site. The EC_{50} data from both roscovitine and nonroscovitine datasets (A) were normalized to the EC_{50} value at 0 mV (for each dataset; B) and fit using the Woodhull equation (Eq. 1) to yield an electrical distance of ∼0.55. The data at V < 0 mV were not included in the fit.

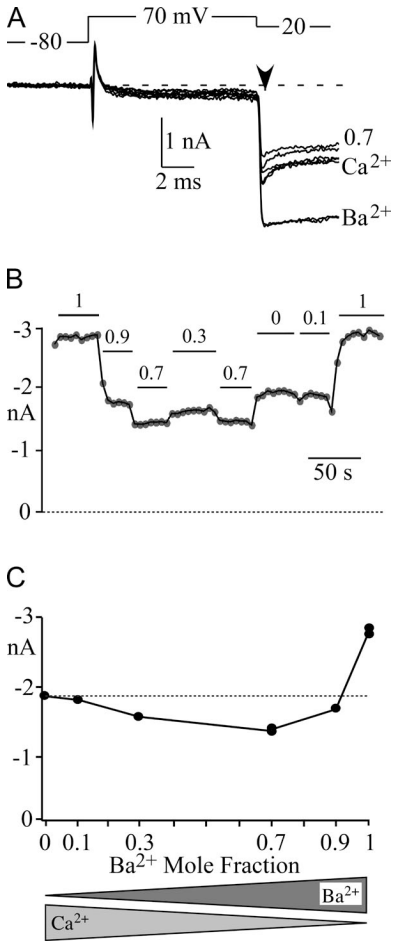

Figure 8. AMFE in N-type channels. (A) This voltage-clamped neuron produced a small inward current at 70 mV (step) and a large tail current measured at 20 mV. [Ba^{2+}] + [Ca^{2+}] was held at 10 mM throughout, but the fractions of each were changed. Ba^{2+} currents were larger than Ca^{2+}. The value 0.7 indicates [Ba^{2+}]/([Ba^{2+}] + [Ca^{2+}]) = 0.7 and is the fraction giving the smallest tail current. Tail currents were measured at the arrowhead to yield the time course in B. (B) The time course of an experiment changing the MFs at the times indicated by the horizontal bars. The dashed line is zero current. (C) The mean values of tail current plotted versus MF from the data in B. The relative Ca^{2+} and Ba^{2+} levels are illustrated below.

The Ca^{2+} and Ba^{2+} currents are also equal amplitude at 40 mV in 10 mM divalent cations (Fig. 10). Thus, at some voltages and divalent cation concentrations, Ca^{2+} will produce larger currents than Ba^{2+}.

Adding a fourth site to the model reproduces AMFE

Using the three-site model of Dang and McCleskey (1998), we were able to reproduce our current versus $[Ca^{2+}]_o$ relationships at voltages ≥0 mV. To simulate AMFE, we needed parameters for Ba^{2+} permeation and block, which we obtained from the literature. We used 23.5 mM as the EC_{50} for Ba^{2+} permeation at 0 mV (Zhou and Jones, 1995) and 3 μM for the EC_{50} of block at 0 mV (Liang and Elmslie, 2002). Adding these Ba^{2+} parameters to our three-site step model, we were unable to adequately fit our AMFE data (not depicted). To improve the correspondence between the simulated and experimental data, we altered the well depths, barrier heights, and electrical distances. However, we were never able to fit the data at all concentrations and all voltages using a single set of parameters (Fig. 10 A). A set of parameters that closely reproduces the data at 30 mM severely underestimated the AMFE at lower divalent cation concentrations (Fig. 10 A). In contrast, if we fit the data at 3 mM, the model produced too much AMFE at higher divalent cation concentrations.

The failure to reproduce our AMFE data at all concentrations and voltages suggested that additional model adjustments were needed. We reasoned that to deepen the AMFE at lower ionic concentrations, we would add at least one binding site. This new site needed to accomplish two tasks. The first was to deepen the Ca^{2+} block of Ba^{2+} current at low divalent cation concentrations (i.e., stronger AMFE at 3 mM). The second was to increase the relative Ba^{2+} current at depolarized voltages in high divalent cation concentrations (i.e., 40 mV at 30 mM; Fig. 10 A). The new site was added to the extracellular side of the pore and was given the same affinity for Ca^{2+} and Ba^{2+} to limit the number of additional free parameters. Using the parameters listed in the Fig. 10 legend, we were able to reproduce the concentration and voltage dependence of AMFE (Fig. 10 B). The failure of the three-site model along with the success of the four-site model supports the involvement of four Ca^{2+}-binding sites in permeation of $Ca_V2.2$ channels.

DISCUSSION

In this study we investigated the voltage dependence of calcium channel block, permeation, and AMFE using electrophysiological recordings and modeling. We found that (a) $Ca_V2.2$ channel block, permeation, and AMFE are all voltage dependent, (b) the voltage dependence of permeation is very strong at depolarized voltages but minimal at voltages <0 mV, (c) the voltage dependence of AMFE required the addition of a fourth site to our model, and (d) there are conditions in which Ca^{2+} currents are larger than, or equal to, Ba^{2+} currents.

Voltage dependence of permeation

Studying $Ca_V1.2$ channels, Kuo and Hess (1993a) found no difference in the EC_{50} for Ba^{2+} permeation at −20 and −40 mV. In addition, Polo-Parada and Korn (1997) suggested there is no voltage dependence to a site external to the high-affinity blocking site of $Ca_V2.2$ channels. These measurements were confined to hyperpolarized voltages (<0 mV) and were consistent with a theoretical study that showed little or no effect of voltage on permeation at voltages <0 mV but larger effects at voltages ≥0 mV (Campbell et al., 1988). Our results expand the voltage range of both experimental and theoretical studies to reveal a strong voltage dependence of permeation that was only apparent at voltages ≥0 mV.

Recent studies of $Ca_V3.1$ current showed little or no voltage dependence of permeation at voltages up to 30 mV (Khan et al., 2008), which was reproduced by a two-well–three-barrier model (Lopin et al., 2010). Although the apparent absence of voltage effects on permeation is

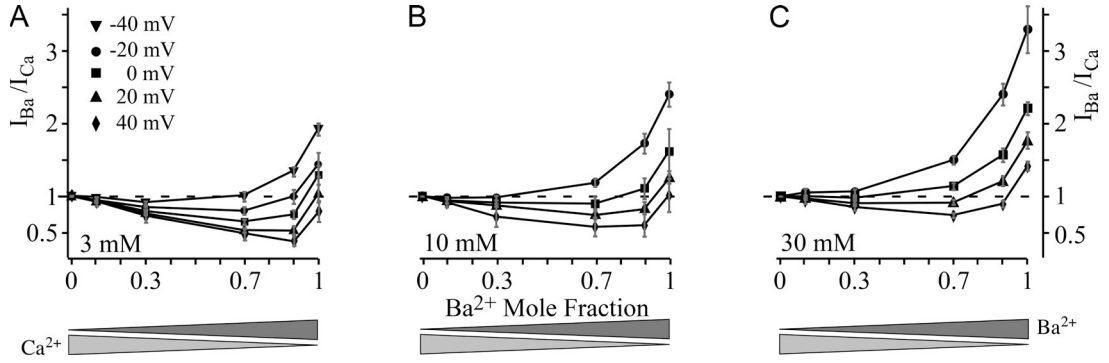

Figure 9. AMFE is voltage and concentration dependent. (A–C) The current measured from tail currents was normalized to that in 100% Ca^{2+} (dashed line) and plotted versus Ba^{2+} MF. The data were recorded at the voltages (symbols) indicated. Note that the current in 3 mM Ba^{2+} (A) at 40 mV (diamonds) is smaller than that in 3 mM Ca^{2+}. The number of neurons recorded was $n = 6$–10 for 3 mM (A), $n = 3$–9 for 10 mM (B), and $n = 4$–10 for 30 mM (C) divalent cations. The relative Ca^{2+} and Ba^{2+} levels are illustrated below.

similar to findings from $Ca_V1.2$ and $Ca_V2.2$ channels, there are clear differences in the data from voltages >0 mV between $Ca_V2.2$ and $Ca_V3.1$ channels. We find a robust increase in the apparent EC_{50} over these voltages (Fig. 5), whereas the data from $Ca_V3.1$ channels are basically flat over the same voltage range (Khan et al., 2008). The reason for this difference is not clear, but it is notable that the presumed selectivity filter of $Ca_V3.1$ channels has two aspartates and two glutamates compared with the four glutamates of $Ca_V2.2$ channels (Cens et al., 2007). In addition, differences between the S5 and S6 regions of Ca_V channels have been shown to significantly contribute to differences in permeation (Cibulsky and Sather, 2003).

There are several implications to the effect of voltage on permeation. (a) Slope conductance as a measure of ion channel permeability should be used with caution because it combines permeation across a range of voltages over which the affinity of the channel for the permeating ions could be changing. Thus, changes in binding site affinity with voltage, along with driving force, determine the slope conductance of a $Ca_V2.2$ channel.

(b) Because Ca^{2+} is a second messenger, it is important to maintain Ca^{2+} influx as much as possible at depolarized voltages even though the driving force is low. The apparent decrease in the affinity of $Ca_V2.2$ channels for Ca^{2+} with voltages >0 mV increases the Ca^{2+} off rate from its binding sites and, thus, Ca^{2+} influx at these depolarized voltages, such as during an action potential. In essence, this mechanism allows the channel to treat Ca^{2+} at depolarized voltages like it otherwise treats Ba^{2+} (which generally produces larger currents than Ca^{2+}; Fig. 9). Likewise, the affinity of the channel for external Na^+ is expected to become even lower at depolarized voltages to effectively increase the competitiveness of Ca^{2+} to permeate $Ca_V2.2$ channels. The relatively increased Ca^{2+} influx from this mechanism may be important for delivering sufficient and consistent Ca^{2+} to trigger neurotransmitter release (Gentile and Stanley, 2005). If $Ca_V1.2$ channel permeation is also voltage dependent (Friel and Tsien, 1989), this mechanism could be critical to delivering Ca^{2+} during the plateau phase of the cardiac action potential. This channel mechanism along with the recently proposed nanodomains that severely restrict

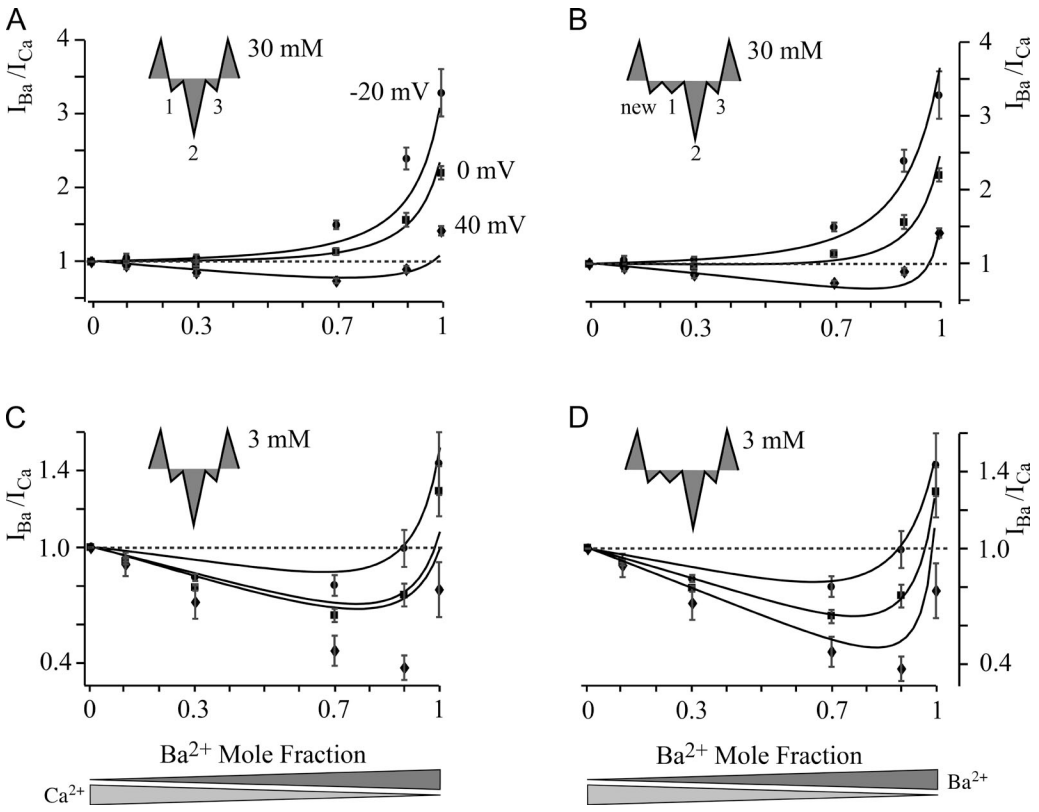

Figure 10. The AMFE data are reproduced by the four-site model. All four panels show experimental Ba^{2+}/Ca^{2+} MF data at different tail voltages (symbols). Total divalent cation concentration (Ba^{2+} + Ca^{2+}) = 30 mM is in A and B and 3 mM is in C and D. (A and C) Simulations (smooth lines) using the three-site model (insets). The well electrical distances were 0.35, 0.5, and 0.65. For Ba^{2+} and Ca^{2+}, respectively, the three wells were −2.65, −12.75, and −2.65 and −4.6, −15, and −4.6 kT deep and the four barriers were 8.6, −0.7, −0.7, and 9.6 and 8.6, −1, −1, and 9.6 kT high. (B and D) The same data were fit with the four-site model with well positions at 0.1, 0.2, 0.5, and 0.9. For Ba^{2+} and Ca^{2+}, respectively, the four wells were −3.5, −1, −12.3, and −2.5 and −3.5, −4.6, −14.7, and −4.6 kT deep, while the five barriers were 8.6, −0.7, −0.7, −0.7, and 9.6 and 8.6, −1, −1, −1, and 9.6 kT high. The relative Ca^{2+} and Ba^{2+} levels are illustrated below C and D.

calcium diffusion (Tadross et al., 2013), together, could ensure sufficient Ca^{2+} levels needed to maintain activation of Ca^{2+}-binding proteins that are coupled to Ca_V channels, without causing Ca^{2+} overload.

(c) The affinity of $Ca_V2.2$ channels for Ca^{2+} changes little at voltages <0 mV, which helps to maintain the influx of Ca^{2+} at hyperpolarized voltages. If the affinity for Ca^{2+} became too high at these hyperpolarized voltages, Ca^{2+} would become a blocking ion instead of a permeating ion. Thus, the limited effect of voltage at hyperpolarized voltage helps, along with driving force, to keep Ca^{2+} influx high.

AMFE

The measurement of AMFE in Ca_V channels has helped to shape the idea that permeation of these channels involves multiple ions moving through the pore in single file (Almers and McCleskey, 1984; Hess and Tsien, 1984). AMFE has been most often studied in L-type ($Ca_V1.2$) channels (Almers and McCleskey, 1984; Hess and Tsien, 1984; Friel and Tsien, 1989; Wang et al., 2005), but one study used voltage steps to demonstrate a small Ca^{2+}-Ba^{2+} AMFE in $Ca_V2.2$ channels (Wakamori et al., 1998).

We used AMFE to test the voltage dependence of permeation and provide an independent dataset by which to test our permeation model. The concentration and voltage dependence of permeation was clearly evident in our AMFE results. This supports previous work by Friel and Tsien (1989), who demonstrated using $Ca_V1.2$ channels that AMFE could be lost at either high divalent cation concentrations or hyperpolarized voltages. Their explanation was that AMFE could only be observed under conditions in which the binding sites within the channels are not saturated. Our results and modeling support this conclusion. At any given voltage, if the affinity of the channel is sufficiently high to bind either species of divalent cation in the mix, then no AMFE will be observed. However, AMFE can be observed either by depolarizing the test voltage (to lower the affinity) or by reducing the divalent cation concentration (to lower the occupancy).

The second reason we performed the AMFE experiments was to test our three-site permeation model. However, after extensive parameter manipulation, we were unable to reproduce our AMFE data using a single set of model parameters, which motivated us to produce a four-site model (see below).

Ca^{2+} current larger than Ba^{2+} current

Na_V channels select by exclusion, like a molecular sieve (Sun et al., 1997). In other words, these channels have energy barriers that are too high to be overcome by larger ions, such as K^+. However, Ca_V channels developed selectivity by having binding sites, or energy wells, that specifically accommodate some but not other ions (Hille, 1992). Because of these binding sites, it is thought that ions with the highest affinity (deeper wells) will have the slowest mobility to yield smaller currents (Hess et al., 1986), which is the explanation for larger Na^+ and Ba^{2+} currents (which have shallower wells) compared with Ca^{2+} currents through Ca_V channels. Remarkably, at depolarized voltages (40 mV) in physiological concentrations of divalent cations ~3 mM, we found that Ca^{2+} currents were larger than Ba^{2+} currents (Fig. 9 A, 40 mV). The explanation is that even though Ba^{2+} binds with a lower affinity than Ca^{2+} to the sites within the pore, at depolarized voltages this affinity becomes so low that multiple occupancy of the channel, required for permeation, is drastically diminished for Ba^{2+}. In contrast, Ca^{2+} binds with a higher affinity than Ba^{2+}, which helps it better maintain multiple occupancy of the channel to generate more current at very depolarized voltages.

Permeation models

Multiple models have been proposed to explain the permeation of Ca^{2+} through $Ca_V1.2$ channels. These include barrier-well models based on Eyring rate theory (Almers and McCleskey, 1984; Hess and Tsien, 1984; Dang and McCleskey, 1998) and models based on Poisson-Nernst-Plank theory (Nonner and Eisenberg, 1998; Rodriguez-Contreras et al., 2002). We chose to investigate the barrier-well models, but our data on the concentration and voltage dependence of $Ca_V2.2$ channel permeation will be useful for testing other models of Ca_V channel permeation.

The original barrier-well permeation models postulated two high-affinity binding sites for divalent cations within the pore (Almers and McCleskey, 1984; Hess and Tsien, 1984). Permeation was achieved in these models by including a mutual repulsion factor that accelerated the exit of divalent cations from the pore. Another version of this model added two low-affinity binding sites to the two high-affinity sites, which helped explain the block of Ca^{2+} flux by internal Li^+ (Kuo and Hess, 1993c). However, these models were abandoned after mutagenesis experiments supported only a single high-affinity site (Yang et al., 1993; Ellinor et al., 1995). In response, Dang and McCleskey (1998) produced the three-site model with only a single high-affinity binding site and two bracketing sites (enhancement sites). The lower affinity of the enhancement sites produced high rates of Ca^{2+} flux by providing steps, or energetically favorable sites, from which ions could leave the pore and, thus, did not require repulsion.

Given the success of the three-site model in reproducing $Ca_V1.2$ channel data, we were interested in testing it on our dataset from $Ca_V2.2$ channels. We were able to identify a set of parameters that would reproduce the voltage and concentration dependence of Ca^{2+} permeation, but we could not find a common set of parameters that would reproduce AMFE across different voltages and divalent cation concentrations. Although we initially

constrained the parameters for the model by experimental measurements, we allowed them to vary in our attempts to reproduce the AMFE data. Again, no single parameter set could be found.

Ions getting into a pore that is already occupied by another ion (in a different site) may or may not encounter repulsion from ions already in the pore (Almers and McCleskey, 1984; Hess and Tsien, 1984). We introduced repulsion into the three-site model in an attempt to improve the correspondence between our simulated and experimental AMFE data. Simply adding repulsion to our model enhanced AMFE at high divalent cation concentrations (Fig. S1), whereas other parameter adjustments minimized AMFE at low concentrations (Fig. S2). Thus, repulsion appeared to make AMFE less concentration dependent, which was opposite of the effect needed to improve the correspondence with our data.

With the failure of repulsion to improve our simulated AMFE data, we added a fourth binding site (well) to the external side of the channel (the loading site; Fig. 11).

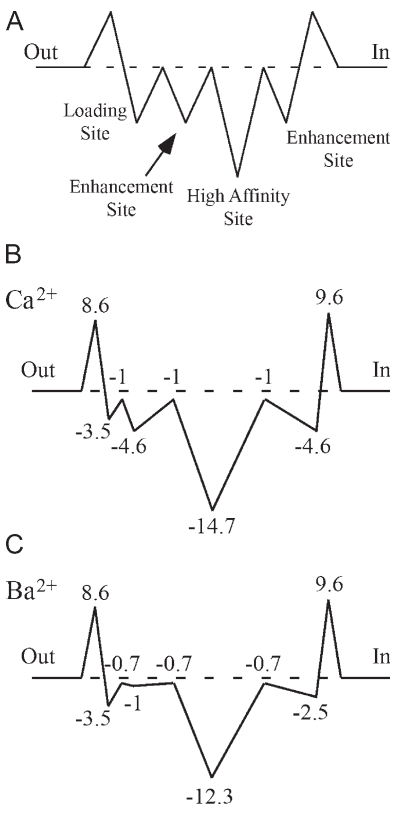

Figure 11. A four-site model of $Ca_V2.2$ channel permeation. (A) A new divalent cation-binding site was added to the three-site model (Fig. 1) at the extracellular side of the pore to satisfy an apparent need for a site that could load ions into the pore (the loading site). The other sites are also labeled. (B) The same model with the barrier heights and well depths showing the values for Ca^{2+}. The wells are also placed at their electrical distances along the pore. Those positions are ∂ = 0.1, 0.2, 0.5, and 0.9. (C) The same model showing the values for Ba^{2+}. The electrical distances are the same as those for Ca^{2+}.

We reasoned that adding a fourth site to the extracellular side of the pore would decrease the occupancy of the external enhancement site, giving rise to a deeper AMFE. Because of its location, we named this site the loading site (Fig. 11).

We were able to reproduce our AMFE data using the four-site model. We set the well depth (i.e., binding affinity) for the loading site to be the same for Ca^{2+} and Ba^{2+} (Fig. 11). Without experimental guidance for setting the parameters for this site, we felt it was best to limit the additional free parameters that would come with the added site. Therefore, a single value for well depth and another for the degree of the transmembrane voltage sensed at the site were the only parameters added to the model. All intrapore barriers were given the same energy value (Fig. 11), which also helped to limit the free parameters for these models.

The addition of the loading site corrected two problems with the three-site model, which were (1) insufficient AMFE at low divalent concentrations and (2) small Ba^{2+} currents (MF = 1) at depolarized voltages (Fig. 11). For the insufficient AMFE at low divalent concentrations, the four-site model increased the depth of AMFE by decreasing the occupancy of the enhancement site by divalent ions that now divide their time between the loading and the enhancement sites. As concluded by Friel and Tsien (1989), AMFE requires that the binding sites within the pore be unsaturated. At low divalent cation concentrations, the loading site allows Ba^{2+} to split its time between the two outside low-affinity wells without leaving the pore, which is energetically less favorable. In contrast, the occupancy of the enhancement site was not sufficiently decreased to prevent permeation. For the second problem, at high divalent cation concentrations and depolarized voltages, the existence of the loading site helps Ba^{2+} increase its occupancy of the enhancement site to create larger Ba^{2+} currents.

The fitting of our AMFE data required adding a fourth site to the model. Unfortunately, structural information is not yet available for any Ca_V channels, so the number of binding sites within the channel is not known. However, a structure was recently obtained from the bacterial Na_V channel that was modified to selectively allow Ca^{2+} permeation (Tang et al., 2014). Interestingly, the structures showed two Ca^{2+}-binding sites bracketing the selectivity filter (presumed high-affinity site), with one or two additional sites at the entrance to the pore. Future structural studies will provide more detailed information, but data from this structure and our modeling are consistent with a Ca^{2+}-selective ion channel having four or perhaps five ion-binding sites along the permeation pathway.

This paper was supported by the Dyson College 2014 Faculty Summer Research Grant Program (Z. Buraei).

The authors declare no competing financial interests.

Sharona E. Gordon served as editor.

Submitted: 27 March 2014
Accepted: 9 July 2014

REFERENCES

Almers, W., and E.W. McCleskey. 1984. Non-selective conductance in calcium channels of frog muscle: calcium selectivity in a single-file pore. *J. Physiol.* 353:585–608.

Almers, W., E.W. McCleskey, and P.T. Palade. 1984. A non-selective cation conductance in frog muscle membrane blocked by micromolar external calcium ions. *J. Physiol.* 353:565–583.

Bidaud, I., A. Mezghrani, L.A. Swayne, A. Monteil, and P. Lory. 2006. Voltage-gated calcium channels in genetic diseases. *Biochim. Biophys. Acta.* 1763:1169–1174. http://dx.doi.org/10.1016/j.bbamcr.2006.08.049

Block, B.M., W.C. Stacey, and S.W. Jones. 1998. Surface charge and lanthanum block of calcium current in bullfrog sympathetic neurons. *Biophys. J.* 74:2278–2284. http://dx.doi.org/10.1016/S0006-3495(98)77937-8

Brink, F. 1954. The role of calcium ions in neural processes. *Pharmacol. Rev.* 6:243–298.

Buraei, Z., M. Anghelescu, and K.S. Elmslie. 2005. Slowed N-type calcium channel (CaV2.2) deactivation by the cyclin-dependent kinase inhibitor roscovitine. *Biophys. J.* 89:1681–1691. http://dx.doi.org/10.1529/biophysj.104.052837

Buraei, Z., G. Schofield, and K.S. Elmslie. 2007. Roscovitine differentially affects CaV2 and Kv channels by binding to the open state. *Neuropharmacology.* 52:883–894. http://dx.doi.org/10.1016/j.neuropharm.2006.10.006

Campbell, D.L., R.L. Rasmusson, and H.C. Strauss. 1988. Theoretical study of the voltage and concentration dependence of the anomalous mole fraction effect in single calcium channels. New insights into the characterization of multi-ion channels. *Biophys. J.* 54:945–954. http://dx.doi.org/10.1016/S0006-3495(88)83030-3

Carbone, E., H.D. Lux, V. Carabelli, G. Aicardi, and H. Zucker. 1997. Ca^{2+} and Na^{+} permeability of high-threshold Ca^{2+} channels and their voltage-dependent block by Mg^{2+} ions in chick sensory neurones. *J. Physiol.* 504:1–15. http://dx.doi.org/10.1111/j.1469-7793.1997.001bf.x

Catterall, W.A., S. Dib-Hajj, M.H. Meisler, and D. Pietrobon. 2008. Inherited neuronal ion channelopathies: new windows on complex neurological diseases. *J. Neurosci.* 28:11768–11777. http://dx.doi.org/10.1523/JNEUROSCI.3901-08.2008

Cens, T., M. Rousset, A. Kajava, and P. Charnet. 2007. Molecular determinant for specific Ca/Ba selectivity profiles of low and high threshold Ca^{2+} channels. *J. Gen. Physiol.* 130:415–425. http://dx.doi.org/10.1085/jgp.200709771

Cibulsky, S.M., and W.A. Sather. 2003. Control of ion conduction in L-type Ca^{2+} channels by the concerted action of S5–6 regions. *Biophys. J.* 84:1709–1719. http://dx.doi.org/10.1016/S0006-3495(03)74979-0

Dang, T.X., and E.W. McCleskey. 1998. Ion channel selectivity through stepwise changes in binding affinity. *J. Gen. Physiol.* 111:185–193. http://dx.doi.org/10.1085/jgp.111.2.185

Ellinor, P.T., J. Yang, W.A. Sather, J.F. Zhang, and R.W. Tsien. 1995. Ca^{2+} channel selectivity at a single locus for high-affinity Ca^{2+} interactions. *Neuron.* 15:1121–1132. http://dx.doi.org/10.1016/0896-6273(95)90100-0

Elmslie, K.S. 1997. Identification of the single channels that underlie the N-type and L-type calcium currents in bullfrog sympathetic neurons. *J. Neurosci.* 17:2658–2668.

Elmslie, K.S., P.J. Kammermeier, and S.W. Jones. 1992. Calcium current modulation in frog sympathetic neurones: L-current is relatively insensitive to neurotransmitters. *J. Physiol.* 456:107–123.

Elmslie, K.S., P.J. Kammermeier, and S.W. Jones. 1994. Reevaluation of Ca^{2+} channel types and their modulation in bullfrog sympathetic neurons. *Neuron.* 13:217–228. http://dx.doi.org/10.1016/0896-6273(94)90471-5

Fabiato, A., and F. Fabiato. 1979. Calculator programs for computing the composition of the solutions containing multiple metals and ligands used for experiments in skinned muscle cells. *J. Physiol. (Paris).* 75:463–505.

Friel, D.D., and R.W. Tsien. 1989. Voltage-gated calcium channels: direct observation of the anomalous mole fraction effect at the single-channel level. *Proc. Natl. Acad. Sci. USA.* 86:5207–5211. http://dx.doi.org/10.1073/pnas.86.13.5207

Gentile, L., and E.F. Stanley. 2005. A unified model of presynaptic release site gating by calcium channel domains. *Eur. J. Neurosci.* 21:278–282. http://dx.doi.org/10.1111/j.1460-9568.2004.03841.x

Goo, Y.S., W. Lim, and K.S. Elmslie. 2006. Ca^{2+} enhances U-type inactivation of N-type (CaV2.2) calcium current in rat sympathetic neurons. *J. Neurophysiol.* 96:1075–1083. http://dx.doi.org/10.1152/jn.01294.2005

Hess, P., and R.W. Tsien. 1984. Mechanism of ion permeation through calcium channels. *Nature.* 309:453–456. http://dx.doi.org/10.1038/309453a0

Hess, P., J.B. Lansman, and R.W. Tsien. 1986. Calcium channel selectivity for divalent and monovalent cations. Voltage and concentration dependence of single channel current in ventricular heart cells. *J. Gen. Physiol.* 88:293–319. http://dx.doi.org/10.1085/jgp.88.3.293

Hille, B. 1992. Ionic Channels of Excitable Membranes. Second edition. Sinauer Associates, Sunderland, MA. 607 pp.

Jones, S.W. 1987. Luteinizing hormone-releasing hormone as a neurotransmitter in bullfrog sympathetic ganglia. *Ann. N. Y. Acad. Sci.* 519:310–322. http://dx.doi.org/10.1111/j.1749-6632.1987.tb36306.x

Jones, S.W. 1990. Whole-cell and microelectrode voltage clamp. In *Neurophysiological techniques: Basic methods and concepts.* Neuromethods. Vol. 14. A.A. Boulton, G.B. Baker, and C.H. Vanderwolf, editors. The Humana Press, Inc., Clifton, New Jersey. 143–192.

Jones, S.W., and T.N. Marks. 1989. Calcium currents in bullfrog sympathetic neurons. I. Activation kinetics and pharmacology. *J. Gen. Physiol.* 94:151–167. http://dx.doi.org/10.1085/jgp.94.1.151

Khan, N., I.P. Gray, C.A. Obejero-Paz, and S.W. Jones. 2008. Permeation and gating in $Ca_V3.1$ (α1G) T-type calcium channels effects of Ca^{2+}, Ba^{2+}, Mg^{2+}, and Na^{+}. *J. Gen. Physiol.* 132:223–238. http://dx.doi.org/10.1085/jgp.200809986

Kuffler, S.W., and T.J. Sejnowski. 1983. Peptidergic and muscarinic excitation at amphibian sympathetic synapses. *J. Physiol.* 341:257–278.

Kuo, C.C., and P. Hess. 1993a. Block of the L-type Ca2+ channel pore by external and internal Mg2+ in rat phaeochromocytoma cells. *J. Physiol.* 466:683–706.

Kuo, C.C., and P. Hess. 1993b. Characterization of the high-affinity Ca2+ binding sites in the L-type Ca2+ channel pore in rat phaeochromocytoma cells. *J. Physiol.* 466:657–682.

Kuo, C.C., and P. Hess. 1993c. Ion permeation through the L-type Ca2+ channel in rat phaeochromocytoma cells: two sets of ion binding sites in the pore. *J. Physiol.* 466:629–655.

Lansman, J.B., P. Hess, and R.W. Tsien. 1986. Blockade of current through single calcium channels by Cd2+, Mg2+, and Ca2+. Voltage and concentration dependence of calcium entry into the pore. *J. Gen. Physiol.* 88:321–347. http://dx.doi.org/10.1085/jgp.88.3.321

Liang, H., and K.S. Elmslie. 2001. E(f)-current contributes to whole-cell calcium current in low calcium in frog sympathetic neurons. *J. Neurophysiol.* 86:1156–1163.

Liang, H., and K.S. Elmslie. 2002. Rapid and reversible block of N-type calcium channels (CaV 2.2) by omega-conotoxin GVIA in the absence of divalent cations. *J. Neurosci.* 22:8884–8890.

Liang, H., C.D. DeMaria, M.G. Erickson, M.X. Mori, B.A. Alseikhan, and D.T. Yue. 2003. Unified mechanisms of Ca^{2+} regulation across the Ca^{2+} channel family. *Neuron.* 39:951–960. http://dx.doi.org/10.1016/S0896-6273(03)00560-9

Liao, P., and T.W. Soong. 2010. $Ca_V1.2$ channelopathies: from arrhythmias to autism, bipolar disorder, and immunodeficiency. *Pflugers Arch.* 460:353–359. http://dx.doi.org/10.1007/s00424-009-0753-0

Lopin, K.V., C.A. Obejero-Paz, and S.W. Jones. 2010. Evaluation of a two-site, three-barrier model for permeation in $Ca_V3.1$ (α1G) T-type calcium channels: Ca^{2+}, Ba^{2+}, Mg^{2+}, and Na^{+}. *J. Membr. Biol.* 235:131–143. http://dx.doi.org/10.1007/s00232-010-9264-3

Martell, A., and R.M. Smith. 1974. *Amino acids.* Critical Stability Constants. Vol. 1. Plenum Press, New York.

Nonner, W., and B. Eisenberg. 1998. Ion permeation and glutamate residues linked by Poisson-Nernst-Planck theory in L-type calcium channels. *Biophys. J.* 75:1287–1305. http://dx.doi.org/10.1016/S0006-3495(98)74048-2

Polo-Parada, L., and S.J. Korn. 1997. Block of N-type calcium channels in chick sensory neurons by external sodium. *J. Gen. Physiol.* 109:693–702. http://dx.doi.org/10.1085/jgp.109.6.693

Rajakulendran, S., D. Kaski, and M.G. Hanna. 2012. Neuronal P/Q-type calcium channel dysfunction in inherited disorders of the CNS. *Nat. Rev. Neurol.* 8:86–96. http://dx.doi.org/10.1038/nrneurol.2011.228

Rodriguez-Contreras, A., W. Nonner, and E.N. Yamoah. 2002. Ca^{2+} transport properties and determinants of anomalous mole fraction effects of single voltage-gated Ca^{2+} channels in hair cells from bullfrog saccule. *J. Physiol.* 538:729–745. http://dx.doi.org/10.1113/jphysiol.2001.013312

Rosenberg, R.L., and X.H. Chen. 1991. Characterization and localization of two ion-binding sites within the pore of cardiac L-type calcium channels. *J. Gen. Physiol.* 97:1207–1225. http://dx.doi.org/10.1085/jgp.97.6.1207

Schmunk, G., and J.J. Gargus. 2013. Channelopathy pathogenesis in autism spectrum disorders. *Front. Genet.* 4:222. http://dx.doi.org/10.3389/fgene.2013.00222

Sun, Y.-M., I. Favre, L. Schild, and E. Moczydlowski. 1997. On the structural basis for size-selective permeation of organic cations through the voltage-gated sodium channel. Effect of alanine mutations at the DEKA locus on selectivity, inhibition by Ca^{2+} and H^{+}, and molecular sieving. *J. Gen. Physiol.* 110:693–715. http://dx.doi.org/10.1085/jgp.110.6.693

Tadross, M.R., R.W. Tsien, and D.T. Yue. 2013. Ca^{2+} channel nanodomains boost local Ca^{2+} amplitude. *Proc. Natl. Acad. Sci. USA.* 110:15794–15799. http://dx.doi.org/10.1073/pnas.1313898110

Tang, L., T.M. Gamal El-Din, J. Payandeh, G.Q. Martinez, T.M. Heard, T. Scheuer, N. Zheng, and W.A. Catterall. 2014. Structural basis for Ca^{2+} selectivity of a voltage-gated calcium channel. *Nature.* 505:56–61. http://dx.doi.org/10.1038/nature12775

Thévenod, F., and S.W. Jones. 1992. Cadmium block of calcium current in frog sympathetic neurons. *Biophys. J.* 63:162–168. http://dx.doi.org/10.1016/S0006-3495(92)81575-8

Wakamori, M., M. Strobeck, T. Niidome, T. Teramoto, K. Imoto, and Y. Mori. 1998. Functional characterization of ion permeation pathway in the N-type Ca2+ channel. *J. Neurophysiol.* 79:622–634.

Wang, X., T.A. Ponoran, R.L. Rasmusson, D.S. Ragsdale, and B.Z. Peterson. 2005. Amino acid substitutions in the pore of the $Ca_V1.2$ calcium channel reduce barium currents without affecting calcium currents. *Biophys. J.* 89:1731–1743. http://dx.doi.org/10.1529/biophysj.104.058875

Woodhull, A.M. 1973. Ionic blockage of sodium channels in nerve. *J. Gen. Physiol.* 61:687–708. http://dx.doi.org/10.1085/jgp.61.6.687

Yang, J., P.T. Ellinor, W.A. Sather, J.F. Zhang, and R.W. Tsien. 1993. Molecular determinants of Ca^{2+} selectivity and ion permeation in L-type Ca^{2+} channels. *Nature.* 366:158–161. http://dx.doi.org/10.1038/366158a0

Yarotskyy, V., and K.S. Elmslie. 2009. Open-state occupancy prevents gating charge relaxation of N-type (CaV2.2) calcium channels. *Biophys. J.* 97:2446–2455. http://dx.doi.org/10.1016/j.bpj.2009.08.014

Yue, D.T., and E. Marban. 1990. Permeation in the dihydropyridine-sensitive calcium channel. Multi-ion occupancy but no anomalous mole-fraction effect between Ba2+ and Ca2+. *J. Gen. Physiol.* 95:911–939. http://dx.doi.org/10.1085/jgp.95.5.911

Zamponi, G.W., E. Bourinet, and T.P. Snutch. 1996. Nickel block of a family of neuronal calcium channels: subtype- and subunit-dependent action at multiple sites. *J. Membr. Biol.* 151:77–90. http://dx.doi.org/10.1007/s002329900059

Zhou, W., and S.W. Jones. 1995. Surface charge and calcium channel saturation in bullfrog sympathetic neurons. *J. Gen. Physiol.* 105:441–462. http://dx.doi.org/10.1085/jgp.105.4.441